Chemical Engineering Journal 155 (2009) 474–482

Contents lists available at ScienceDirect

Chemical Engineering Journal

journal homepage: www.elsevier.com/locate/cej

Ni-based supported catalysts from layered double hydroxides: Tunable microstructure and controlled property for the synthesis of carbon nanotubes

Lu Zhang, Feng Li*, Xu Xiang, Min Wei, David G. Evans

State Key Laboratory of Chemical Resource Engineering, Beijing University of Chemical Technology, P.O. Box 98, Beijing 100029, PR China

ARTICLE INFO

Article history:
Received 12 April 2009
Received in revised form 1 July 2009
Accepted 3 July 2009

Keywords:
Carbon nanotubes
Layered double hydroxide
Catalyst
Helical
Growth
Microstructure

ABSTRACT

The carbon nanotubes (CNTs) with straight and helical nanostructures have been synthesized by catalytic chemical vapor deposition of acetylene over a series of Ni-based supported catalysts, which were formed from Ni–Mg–Al layered double hydroxide precursors (LDHs) synthesized through homogenous decomposition of urea under hydrothermal conditions. The materials were characterized by power X-ray diffraction (XRD), scanning electron microscope (SEM), transmission electron microscope (TEM), temperature-programmed reduction experiments (TPR), X-ray photoelectron spectroscopy (XPS) and Raman spectroscopy. The results showed that the introduction of Mg into Ni-based supported catalysts could effectively improve the catalytic activities for the growth of CNTs, mainly proceeding from the inhibition effect of spinel phases formed in calcined LDHs on the agglomeration of metallic Ni particles. Furthermore, it is found interestingly that the addition of Mg also could induce the formation of helical structured CNTs with outer diameters of ~20 nm and that the higher Mg content gave rise to the more helical nanotubes. The present work provides a simple and facile way to prepare metal-supported catalysts with a good dispersion of catalytically active metal particles for the growth of straight and helical CNTs.

1. Introduction

Since the landmark findings on the tubular structure of carbon were achieved by Iijima [1], carbon nanotubes (CNTs) have attracted worldwide attention in the past two decades because of not only their fascinating and unique physicochemical properties but also their promising applications in transistors, field-emission tips, sensors, supercapacitors and bio-medical fields [2–6]. On the basis of the sp, sp^2 and sp^3 hybridization of carbon bonding, CNTs can exhibit a variety of shapes including straight, curved, helical and bamboo-shaped ones, which provides the flexibility to tailor the characteristics of carbon structure according to specific needs. In particular, the helical CNTs, which have a diversity of interesting 3D-helical (or spiral) nanotubes with different helical patterns, pitches or diameters, are of great importance for nanoelectromechanical systems and advanced composite materials, etc. [7,8], owing to their excellent electrical, magnetic, electromagnetic and mechanical properties [9].

Of various chemical or physical synthesis techniques, catalytic chemical vapor deposition (CCVD) appears to be the most promising one for large-scale preparation of CNTs. The formation of carbon nanostructures occurs through the catalytic decomposition of a carbonaceous gas on nanosized metal particles, which are transition metals (iron, nickel, cobalt and their alloys) or noble metals supported over high-surface-area materials to disperse and stabilize metallic particles. Many works have been carried out to obtain a good dispersion of metal species on support materials, such as metal oxides, silica and different types of zeolites [10–13]. Generally, nanotubes prepared by CCVD present straight or randomly curled morphologies. However, the helical structured CNTs can be synthesized by controlling the experimental parameters, such as used catalysts, carbon sources, reaction temperatures, gas flow rates and feedstock pressures [14–18]. Among them, the type and character of utilized catalyst is the most important factor in the formation of helical nanostructures. The catalysts act as the seeds for the nucleation and growth of nanotubes by controlling the overall reactions with the hydrocarbon source, which involves the decomposition, diffusion and precipitation of carbon species. In recent years, the issue on the synthesis of helical CNTs has greatly increased due to their importance in both understanding the experimental fundamentals and extensive use. Therefore, it is very necessary to clarify the influence of the catalyst compositions on the morphologies of CNTs obtained.

Layered double hydroxides (LDHs), also known as anionic clay with brucite ($Mg(OH)_2$)-like structure, consist of positively charged layers and negative anions in the interlayer [19]. The structural versatility of LDHs has been achieved by varying divalent or trivalent metal cations in the layers and the anions intercalated into the

* Corresponding author. Tel.: +86 10 64451226; fax: +86 10 64425385.
E-mail address: lifeng_70@163.com (F. Li).

1385-8947/$ – see front matter © 2009 Elsevier B.V. All rights reserved.
doi:10.1016/j.cej.2009.07.001

interlamellar galleries [20–23]. Thus, highly dispersed metal particles over oxides matrix can be obtained by designing an appropriate LDH precursor containing the desired metal cations and subsequent thermal treatment followed by reduction, originating from the ordered prearrangement of metal cations in the layers of LDH precursor at an atomic level. For instance, we recently have shown that it is easy for the supported metallic cobalt catalysts derived from LDH materials to obtain a good size control of catalytic metal particles at a nanometer scale, which is crucial for the growth of CNTs [24,25].

As compared to other powder-supported materials, metal-based supported catalysts achieved from the LDH precursor materials are advantageous to the preparation of CNTs, owing to their large surface area, high dispersion of metals and low cost. However, to the best of our knowledge, no other previous work was reported in detail on the synthesis of CNTs with helical structures over calcined LDHs by the CCVD method. In the present work, we report an alternative method for synthesizing CNTs with straight and helical morphologies by nickel-catalyzed chemical vapor deposition of acetylene. A series of novel Ni-based supported catalysts derived from LDHs containing Ni^{2+}, Mg^{2+} and Al^{3+} cations were prepared homogeneously via urea decomposition under hydrothermal conditions. The effect of compositions of catalysts on the growth of final CNT products was elucidated in detail. It is found that the morphology of the CNTs mainly depended on the catalysts and the growth of regular helical CNTs was observed in the presence of the highly Mg-containing catalyst, suggesting that the Mg element plays an important role on the formation of the helical nanostructures. Furthermore, the growth mechanism of CNTs was also discussed.

2. Experimental

2.1. Preparation of LDH precursors

Layered double hydroxides containing M(II) and M(III) cations (M(II) = Ni^{2+} and Mg^{2+}, M(III) = Al^{3+}) were synthesized under hydrothermal conditions through homogenous decomposition of urea. In a typical synthesis, urea, $Ni(NO_3)_2{\cdot}6H_2O$, $Mg(NO_3)_2{\cdot}6H_2O$ and $Al(NO_3)_3{\cdot}7H_2O$ with the $(Ni^{2+} + Mg^{2+})/Al^{3+}$ molar ratio of 2.0 and Mg^{2+}/Ni^{2+} molar ratio of X (X = 0, 0.5, 1, 2) were dissolved in 80 mL of deionized water to present a clear solution with the total cation concentration of 0.05 M. Here, the molar ratio of urea to total cations is 3.3. Then the aqueous solution was transferred to 100 mL of Teflon-lined autoclave and heated at 150 °C for 24 h. The suspension was washed with deionized water four times and the obtained solid was dried at 70 °C for 12 h in air. The as-synthesized LDH sample (here designed as LDH-X) was calcined in air at 700 °C for 2 h at a heating rate of 5 °C/min. At last, the resulting mixed metal oxides were slowly cooled to room temperature.

2.2. Growth of CNTs

CNTs were synthesized in a quartz tube inside a horizontal tube furnace equipped with mass controller and temperature-programmed control by catalytic chemical vapor deposition of acetylene (C_2H_2). After loading the calcined LDH samples in an alumina boat, the furnace was firstly raised to 500 °C with 5 °C/min under nitrogen gas flow (flow rate: 60 standard-state $cm^3\ min^{-1}$ (sccm)). When reaching 500 °C, H_2 gas (6 sccm) was introduced and the temperature was maintained for 40 min. Subsequently, H_2 gas was switched off and the furnace was further heated to 700 °C, before C_2H_2 gas was switched on with a flow rate of 6 sccm. The temperature was maintained at 700 °C for 60 min. After the reaction, N_2 gas was continued till the furnace was cooled to room temperature. The resultant black powder was collected from the boat. The yield of carbon materials containing CNTs was calculated as follows: yield (%) = (mass of carbon materials deposited onto the catalyst/the initial mass of mixed oxide) × 100.

Table 1
Analytical and structural data for the Ni/Mg/Al-LDHs in the synthesis mixture.

Sample	LDH-0	LDH-0.5	LDH-1	LDH-2
Mg^{2+}/Ni^{2+} ratio	0	1/2	1/1	2/1
$Ni^{2+}/(M^{2+} + M^{3+})$ ratio	6/9	4/9	3/9	2/9
Lattice parameter a[a] (nm)	0.3032	0.3039	0.3042	0.3045
Crystallite size in c direction[b] (nm)	16.4	20.5	21.3	24.5

[a] $a = 2d_{110}$.
[b] Calculated using the Scherrer equation.

2.3. Characterization

Powder X-ray diffraction (XRD) patterns of the samples were collected using a Shimadzu XRD-6000 diffractometer under the following conditions: 40 kV, 30 mA, graphite-filtered Cu Kα radiation (λ = 0.15418 nm). The samples were step-scanned in steps of 0.04° (2θ) using a count time of 10 s/step.

Scanning electron microscopy (SEM) microanalyses of the samples were made using a Hitachi S4700 apparatus with the applied voltage of 20 kV, combined with energy dispersive X-ray spectroscopy (EDX) for composition determination.

Temperature-programmed reduction experiments (TPR): The sample (50 mg) was placed in a quartz reactor and reduced in a stream of H_2 (4% H_2 + 96% N_2) with a heating rate of 10 °C/min up to 900 °C and held at this temperature for 20 min. Hydrogen consumption was monitored continuously by a gas chromatograph.

Transmission electron microscopy (TEM) images were taken using Philips FEI TECNAI 20 transmission electron microscope operated at 120 kV. For analysis, a droplet of the ultrasonically dispersed samples in ethanol was placed onto an amorphous carbon-coated copper grid and then dried at atmospheric ambient. High resolution transmission electron microscopy (HRTEM) was carried out at an accelerating voltage of 200 kV.

X-ray photoelectron spectroscopy (XPS) measurements were carried out with a V.G. Scientific ESCALAB Mark II system and Mg Kα ($h\nu$ = 1253.6 eV) as X-ray source. The binding energies (BE) were referenced to the C1s peak at 284.6 eV. The experimental curve was fitted with a program that made use of a combination of Gaussian–Lorentzian lines.

Thermogravimetric analysis (TG) was carried out in air on a HCT-2 thermal analysis system produced locally. Samples of 10.0 mg were heated at a rate of 10 °C/min.

Raman spectra were recorded at room temperature on a microscopic confocal Raman spectrometer (Jobin Yvon Horiba HR800) using an Ar^+ laser of 532 nm wavelength as excitation source. The laser of 10 mW output power was focused on the surface of samples. The sample was measured for ten times at ten different Raman spectrum spots.

3. Results and discussion

3.1. Characterization of LDH precursors

As illustrated in Table 1, four different LDH precursors with the $(Ni^{2+} + Mg^{2+})/Al^{3+}$ molar ratio of 2.0 in the synthesis mixture were employed for the growth of CNTs. Fig. 1 shows the powder XRD patterns of samples. In each case, the XRD patterns exhibit the characteristic reflections of hydrotalcite-like materials [26,27] and no other crystalline phases are present. The XRD patterns give a series of narrow symmetric (0 0 l) peaks at low 2θ angles, corresponding to the basal spacing around 7.7 Å and higher order diffractions. This

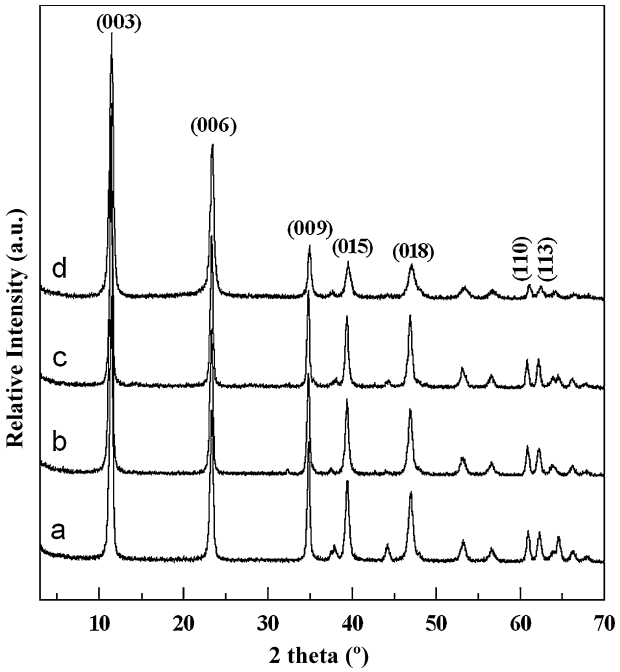

Fig. 1. XRD patterns of LDH samples. (a) LDH-0, (b) LDH-0.5, (c)LDH-1 and (d) LDH-2.

result illustrates that the samples consist of a well-crystallized single phase. Moreover, note that compared with Mg-free sample, the intensity of (0 0 *l*) characteristic peak decreases gradually with the partial replacement of nickel by magnesium into the octahedral coordination environment of brucite-like layers, indicative of the decrease in structural integrality. Assuming a three-layer rhombohedral (3R) stacking of the layers, the lattice parameter *a* represents the mean cation–cation distance within the layer ($=2d_{1\,1\,0}$) [28]. As for LDH phase, it can be noted from Table 1 that the replacement of nickel with magnesium leads to an increase in lattice parameter *a* from 0.3032 to 0.3045 nm, reflecting the fact that the ionic radii for Ni^{2+} and Mg^{2+} are 0.070 and 0.072 nm, respectively. In addition, the coherent diffraction domain size of the LDH in the *c* direction (the stacking direction, perpendicular to the layers) may be estimated from the values of the fullwidth at half-maximum (FWHM) of the main (0 0 3), (0 0 6) and (0 0 9) reflections by means of the Scherrer equation [$=0.89\lambda/\beta(\theta)\cos\theta$] [29], where λ is the wavelength of the radiation used (0.15418 nm), θ is the Bragg diffraction angle and $\beta(\theta)$ is obtained as difference of the sample width profile (FWHM) and the instrumental contribution. With the increase of the Mg content, the estimated coherent diffraction domain size for the samples increases from 16.4 to 25.4 nm (Table 1), suggesting that the introduction of divalent cation with larger ionic radius is advantageous to the stacking of the layers.

Fig. 2 shows SEM images of four LDH precursors. It is seen that in each case the sample is composed of well-defined plate-like particles with rounded edges, a thickness of 15–20 nm and a lateral dimension mainly ranging from 200 to 250 nm, although some smaller particles are still observed. The plate-shaped morphology is commonly observed in four LDH products and less significantly changed by hydrothermal treatments, indicative of uniformity of the product with well-crystalline structure. Usually, urea can hydrolyze slowly under the hydrothermal treatment, leading to simultaneous nucleation and aging passing, which is advantageous to the growth of brucite-like layers and thus large crystallites.

3.2. Characterization of calcined LDHs and CNTs

The XRD patterns of CNT products over calcined LDHs are shown in Fig. 3. The peak centered at about 26.1° can be indexed to (0 0 2) reflection plane of graphite, confirming the existence of carbon. Meanwhile, the (1 1 1), (2 0 0) and (2 2 0) reflections of metallic Ni

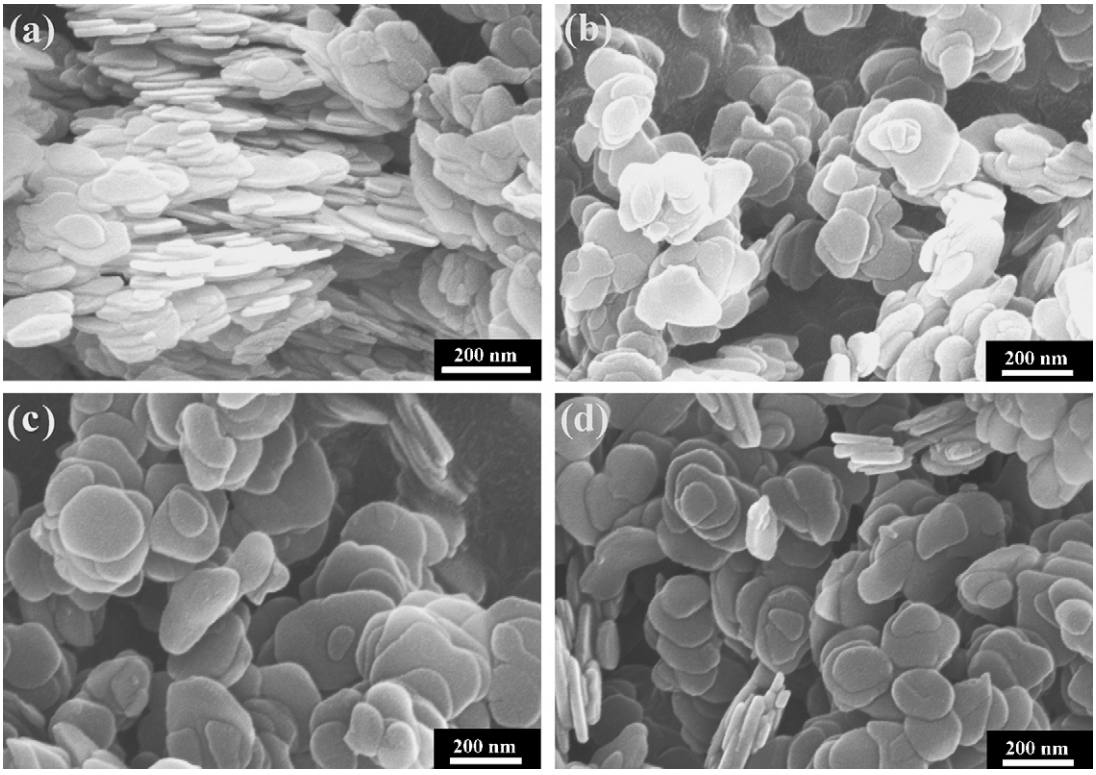

Fig. 2. SEM images of samples. (a) LDH-0, (b) LDH-1, (c) LDH-1 and (d) LDH-2.

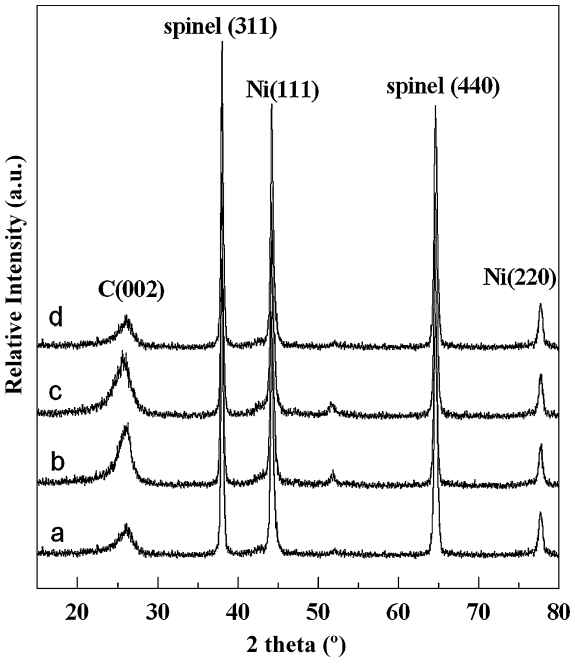

Fig. 3. XRD patterns of CNTs over calcined LDH-0 (a), LDH-0.5 (b), LDH-1 (c) and LDH-2 (d).

appear at 44.2°, 51.5° and 77.8°, respectively, in agreement with those of face-centered cubic (fcc) Ni phase (JCPDS No. 87-0712). Additionally, the intensive peaks at 38.0° and 65.5° correspond to (3 1 1) and (4 4 0) reflection planes of crystalline spinel phase, respectively. It is thought that calcination of LDHs at intermediate temperatures (450–600 °C) or above affords poorly crystalline mixed metal oxides [30], while calcination at 700 °C or above gives spinels, but these are always mixed with the oxide of divalent metal [31]. The above result implies that divalent Ni species in the form of metal oxide can be completely reduced into metallic Ni in the present system, even though a few metallic Ni species may come from difficultly reduced spinel phase in the form of $NiAl_2O_4$ or $Ni_{1-x}Mg_xAl_2O_4$. TPR results of calcined LDH samples (Fig. 4) demonstrate clearly that with the increase in Mg content, the reduction peak temperature of Ni species increases gradually from 703 to 730 °C, mainly owing to the formation of more and more difficultly reduced spinel phases. Correspondingly, the incomplete reduction of Ni^{2+} species favors the dispersion of reduced Ni clusters, thus leading to the formation of small metallic Ni nanoparticles highly dispersed in spinel matrix. According to Scherrer's formula, the crystallite sizes of metallic Ni particles in the (1 1 1) and (2 2 0) directions decrease with increasing Mg content. However, the changes of crystallite sizes in (2 2 0) direction are relatively small (See Table 2). As a result, the spinel phases exhibit a remarkable segregation and inhibition effect on the growth of metallic Ni particles.

Table 2
Crystallite size of Ni particles from the XRD patterns of calcined LDH samples.

Sample	Miller indices (*h k l*)	Crystallite size (nm)
LDH-0	111	28.3
	220	17.0
LDH-0.5	111	21.7
	220	16.5
LDH-1	111	19.5
	220	15.6
LDH-2	111	17.7
	220	15.2

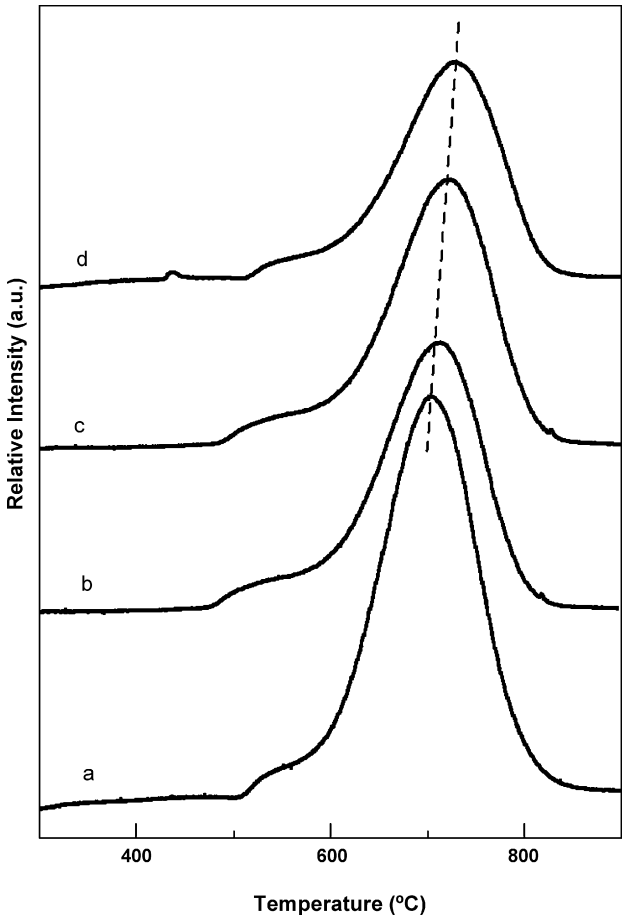

Fig. 4. TPR profiles for calcined LDH-0 (a), LDH-0.5 (b), LDH-1 (c) and LDH-2 (d).

On the other hand, XPS has been applied to determine the chemical states of surface species in calcined LDHs. The Ni $2p_{3/2}$ regions show the presence of four peaks (Fig. 5) in the range of 850–870 eV and their characteristics are given in Table 3. In calcined LDHs, nickel species present in the form of simple metal oxide and spinel phase are confirmed by the XRD patterns. The first peak around 854.8 eV is attributed to Ni^{2+} ions within NiO phase ($Ni_B{}^{2+}$), while the second peak around 856.8 eV is related to Ni^{2+} ions within the spinel structure ($Ni_A{}^{2+}$). Meanwhile, the other two peaks, which lie at ca. 7 eV above the first and second peaks, respectively, are assigned to their corresponding shake-up satellite lines. This means that these peaks appearing at higher BE are assignable to be Ni cations in the stronger interaction sites with near groups in mixed oxides, resulting in the lower reducibility of Ni species. Moreover, according to the proportions of the two chemical states of the Ni^{2+}, taking into account the main peaks as well as their satellite lines (Ni^{2+} sat.) in the Ni $2p_{3/2}$ spectra, a slight trend of enhancement of the ratio of spinel

Table 3
XPS data of Ni $2P_{3/2}$ regions for calcined LDHs.

LDH samples	Binding energy (eV)				Peak intensity (%)	
	$Ni_B{}^{2+}$	$Ni_A{}^{2+}$	$Ni_B{}^{2+}$ sat.	$Ni_A{}^{2+}$ sat.	$I(Ni_B{}^{2+})$[b]	$I(Ni_A{}^{2+})$[a]
LDH-0	854.9	856.9	861.1	863.4	62	38
LDH-0.5	854.9	856.6	861.1	863.5	56	44
LDH-1	854.9	856.4	861.2	863.4	54	46
LDH-2	854.2	856.7	861.2	863.8	50	50

[a] Intensity of the $Ni_A{}^{2+}$ peaks (main peak and sat.) in % of the total Ni $2p_{3/2}$ area.
[b] Intensity of the $Ni_B{}^{2+}$ peaks (main peak and sat.) in % of the total Ni $2p_{3/2}$ area.

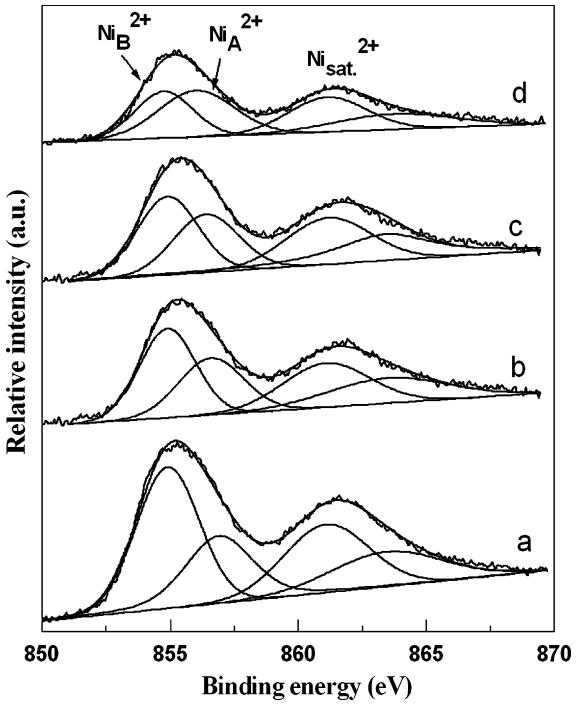

Fig. 5. XPS of Ni $2P_{3/2}$ regions in calcined LDH-0 (a), LDH-0.5 (b), LDH-1 (c) and LDH-2 (d).

phase to NiO can be observed with the increasing Mg content, consistent with the TPR results. It predicts that different compositions of catalysts will directly affect the growth of CNTs.

SEM images of the as-synthesized carbon materials without purification are shown in Fig. 6. From Fig. 6a, only a few CNTs were sporadically observed over calcined LDH-0 sample and the calculated yield of carbon materials is about 109%, because carbon source did not touch sufficiently the large Ni particles obtained during CCVD process. Therefore, the lamella-like morphology of the catalysts was well maintained after reaction. With the introduction of Mg, much more twisting CNT products with small outer diameter of 30–50 nm and the length from several micrometers to tens of micrometers were observed over calcined LDH-0.5 sample in a wide field (Fig. 6b), indicating a high yield of carbon materials (254%). When the Mg/Ni molar ratio in catalyst reached up to 1, it is observed that besides straight CNTs, some solenoid-like helical structured CNTs with different single-helix diameter and helix pitch length were co-grown (Fig. 6c) and that the calculated yield of carbon materials is about 257%. With the further increase of Mg/Ni molar ratio to 2, more and more regular 3D-helical CNTs with different pitches, which are like projected coiling spring, undrawed spring or stretched zigzag-like spring with a node at the cross-region, was observed in Fig. 6d, although the total yield of carbon materials is decreased to 200%. According to thermogravimetric analysis (no shown), the weight loss of carbon materials in the range of 200–400 °C comes from the removal of amorphous carbon because of its lower activation energy for oxidation [32]. Therefore, the weight proportion of amorphous carbon over calcined LDH-0.5, calcined LDH-1 and calcined LDH-2 is about 4.7, 7.1 and 12.4%, respectively. The above results suggest that the Mg element plays an important role on the formation of helical CNTs, mainly due to the fact that the introduction of Mg to the catalyst could tailor the ratio of Ni_A^{2+}/Ni_B^{2+} in calcined LDHs, thus leading to the change in catalyst compositions. However, it is difficult to exactly obtain statistical percentage of helical nanostructure because a large number of CNTs with various morphologies and nanostructures were entangled together.

Fig. 6e–i shows high-magnification SEM images of obtained helix CNTs with various morphologies. In Fig. 6e, a helical nanotube displays stretched zigzag-like shape with a node at the cross-region, while a part of nanotubes show planar-spiral shapes in Fig. 6f. Fig. 6g–i shows another kind of single-helical morphology of nanotubes, similar to solenoid. Especially, the top of the projected coiling shape of the helix nanotubes can be clearly observed in Fig. 6i. In comparison with other morphologies, single-helical nanotubes possess relatively small helical pitches. EDX spectrum of the as-grown CNTs over calcined LDH-2 confirms that the product is mainly composed of carbon (85.4 wt%) and that the atomic ratio of Ni/Mg/Al in sample is very close to 2/4/3, in agreement with the original ratio of metal cations in the synthesis mixture.

TEM studies also give further information about the morphology and structure of CNT products (Fig. 7). It is observed that calcined LDH-0 sample was encapsulated by amorphous carbon and nanotubes are hardly observed, which is consistent with the SEM observation (Fig. 6a). However, note that the products over calcined LDH-0.5 sample have common characteristics of tubular structure with hollow core and little contamination of amorphous carbon (Fig. 7b), confirmed by the above TG result. With the increase of Mg/Ni molar ratio from 1 to 2, more and more helical nanotubes with different shapes (single-helical, planar-spiral and zigzag-like) were observed. Furthermore, with the Mg content, the nanotubes have smaller outer diameter, in good agreement with the change in the size of nanosized Ni particles obtained.

HRTEM images of the CNTs over calcined LDH-0.5 sample have been shown in Fig. 8a and b. It is found that a slender nanoscale particle was encapsulated at the end of nanotube (Fig. 8a), confirming a tip-growth mechanism [33]. The size of the particles along the radial direction of nanotubes was ca. 8 nm, very close to the inner diameter of nanotubes. Although the catalyst particles were commonly observed at one end of the nanotubes, an elliptical nanoparticle inside the nanotubes, which presents the (1 1 1) characteristic planes of fcc Ni phase with an interplanar distance of about 0.203 nm, was also found (Fig. 8b). The above results suggest that the Ni nanoparticles can be elongated along the growth direction of nanotubes due to the weak bondage in this direction. Fig. 8c and d shows locally enlarged images of two individual helical nanotubes with hollow cores and outer diameters of about 10 nm, which were obtained over calcined LDH-2 sample. It reveals that the nanotube consists of more than ten sheets typical of multi-walled nanotubes and that the interlayer spacing of the CNT is about 0.34 nm, almost consistent with the (0 0 2) plane distance of graphite sheets. The amplificatory coiling region clearly exhibited the 2D projection of the coil structure. Different helical shape can be decided by the twist angle and the pitch of elongate tube. For example, Fig. 8e shows the zigzag node, where the graphitic layers are circulating around the center of the node and there is a hollow structure at the center. In addition, note from Fig. 8f that a spherical particle located outside the CNTs was coated by multi-graphite sheets and presents an interplanar distance of about 0.197 nm that is (4 0 0) characteristic plane of spinel phase.

Further structural studies on the as-synthesized CNTs have been achieved by Raman spectra. Taking into account the lack of homogeneity of CNTs samples, ten different Raman spectrum spots have been employed to obtain an average of the spectra. Fig. 9 shows the representative Raman spectra of carbon materials over calcined LDH-0.5 and calcined LDH-2. Two strong bands were observed for two spectra, corresponding to D and G band of carbon. The shift at 1585 cm^{-1}, assigned to G band, is related to the vibration of sp^2-bonded carbon atoms in a two-dimensional hexagonal lattice [34], indicative of the formation of crystalline graphite phase. The D band, at 1349 cm^{-1}, is associated with vibrations of carbon atoms with dangling bonds in plane terminations of disordered graphite or the presence of amorphous carbon [35]. Commonly, the intensity

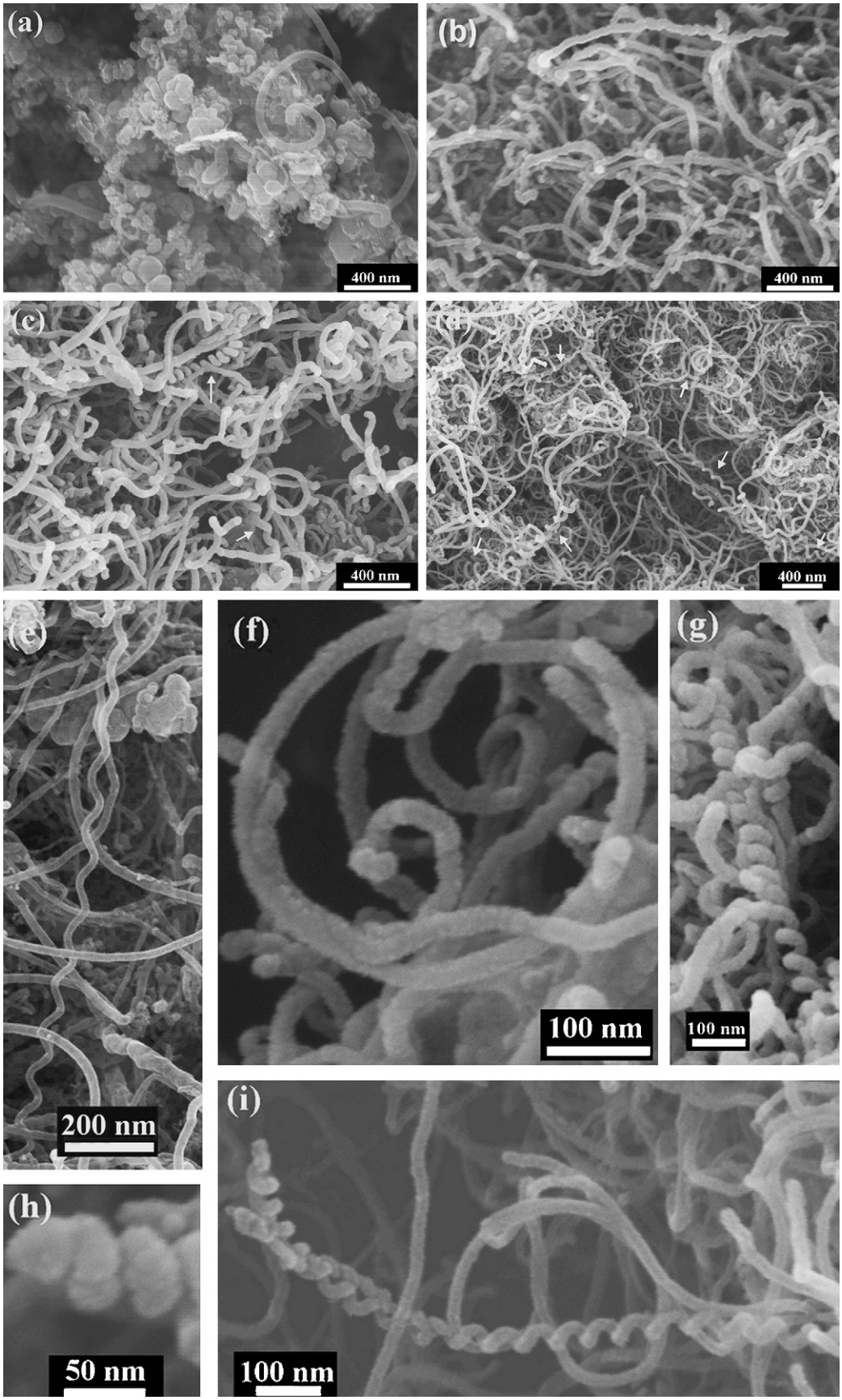

Fig. 6. SEM images of CNTs over calcined LDH-0 (a), LDH-0.5 (b), LDH-1 (c) and LDH-2 (d), and magnified SEM images of several individual helical CNTs with different shapes (e–i).

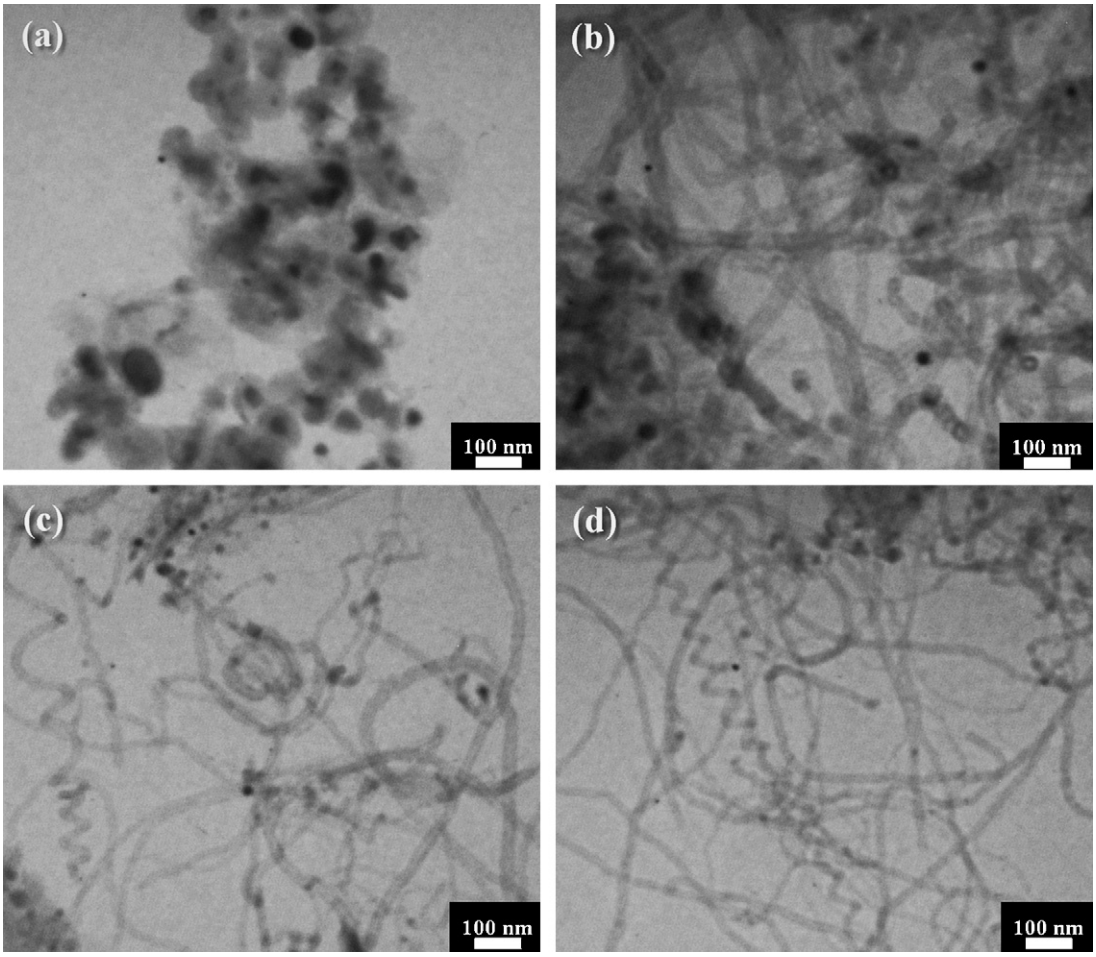

Fig. 7. TEM images of CNTs over calcined LDH-0 (a), LDH-0.5 (b), LDH-1 (c) and LDH-2 (d).

ratio of D band to G band (I_D/I_G) gives the degree of lattice distortion of graphite layer within carbon material. The smaller this value, the higher the crystalline order of graphite phase. It is seen from Fig. 10 that with the increasing Mg^{2+}/Ni^{2+} ratio from 0.5 to 2, the average I_D/I_G values from ten different Raman spectrum spots are calculated to be 0.94 and 1.14, respectively, which originates from the formation of a part of helical CNTs with lower order of graphite layer over calcined LDH-2 sample, indicating a larger quantity of defects in the obtained CNTs' structure.

3.3. Growth mechanism of carbon nanostructures

In the present reaction system, Ni atoms were released from calcined LDHs by reduction at 500 °C and further formed metallic Ni nanoparticles as effective and necessary dehydrogenation catalyst with the increase of temperature. At the high-temperature zone of 700 °C in CCVD, the decomposition process of acetylene around the larger metallic Ni nanoparticles derived from Mg-free precursor gave rise to carbon-surrounded Ni particles. Introducing magnesium into catalysts obviously decreased the size of Ni nanoparticles and made them disperse uniformly. Therefore, the surrounding carbon could transform into a graphite tube through carbon nucleation. Usually, a high surface packing density of Ni particles facilitates the nanotubes to grow along longitude direction, as previously demonstrated for the growth of straight CNTs [36].

The formation of three-dimensional helical structured CNTs should be the result of anisotropic and inhomogeneous properties of each crystal facet of Ni particles for carbon deposition on the crystal faces of the catalyst grain [37,38]. The anisotropy of the catalyst crystal planes can be influenced by various experimental conditions including the catalyst composition, possibly giving rise to pentagonal, hexagonal and heptagonal carbon-rings during the growth of CNTs. It is considered that the pairing of pentagonal–heptagonal (P–H) carbon-rings is essential in forming the helically coiling structures, while hexagon carbon-rings are the key to grow the straight CNTs [39]. Based on an anisotropic mechanism, the straight or irregular-curled CNTs are formed when the anisotropy is low. With the introduction of Mg into catalysts, smaller Ni nanoparticles could highly disperse in the spinel matrix. Therefore, the anisotropy of Ni nanoparticles could be enhanced through masking or deactivating of certain crystal facet among Ni crystal facets by the spinel phase, resulting in the change of the curling-chirality during the growth of CNTs. For example, two crystal facets of Ni nanoparticle catalyst act to grow the zigzag-like structure, while the 3D-spiral structure is formed from three crystal facets of catalyst. On the other hand, the spinel support can also influence the performance of catalyst for the growth of CNTs by an electronic interaction between metal and support interaction, which is a benefit for achieving an exposed catalyst facet.

As a result, the driving force for the formation of helical CNTs is the anisotropy (i.e., carbon deposits on the catalyst crystal facets at different rates) of the catalyst crystal grain, which can be controlled by adjusting the compositions of the catalysts. Furthermore, the regular helical nanostructure can be varied by the alternation of the catalytic anisotropy of the crystal facet, thus causing the curling direction to periodically change. Although the catalytic performance of Ni nanoparticles is explicitly associated to their structure on the basis of the findings presented here, the detailed

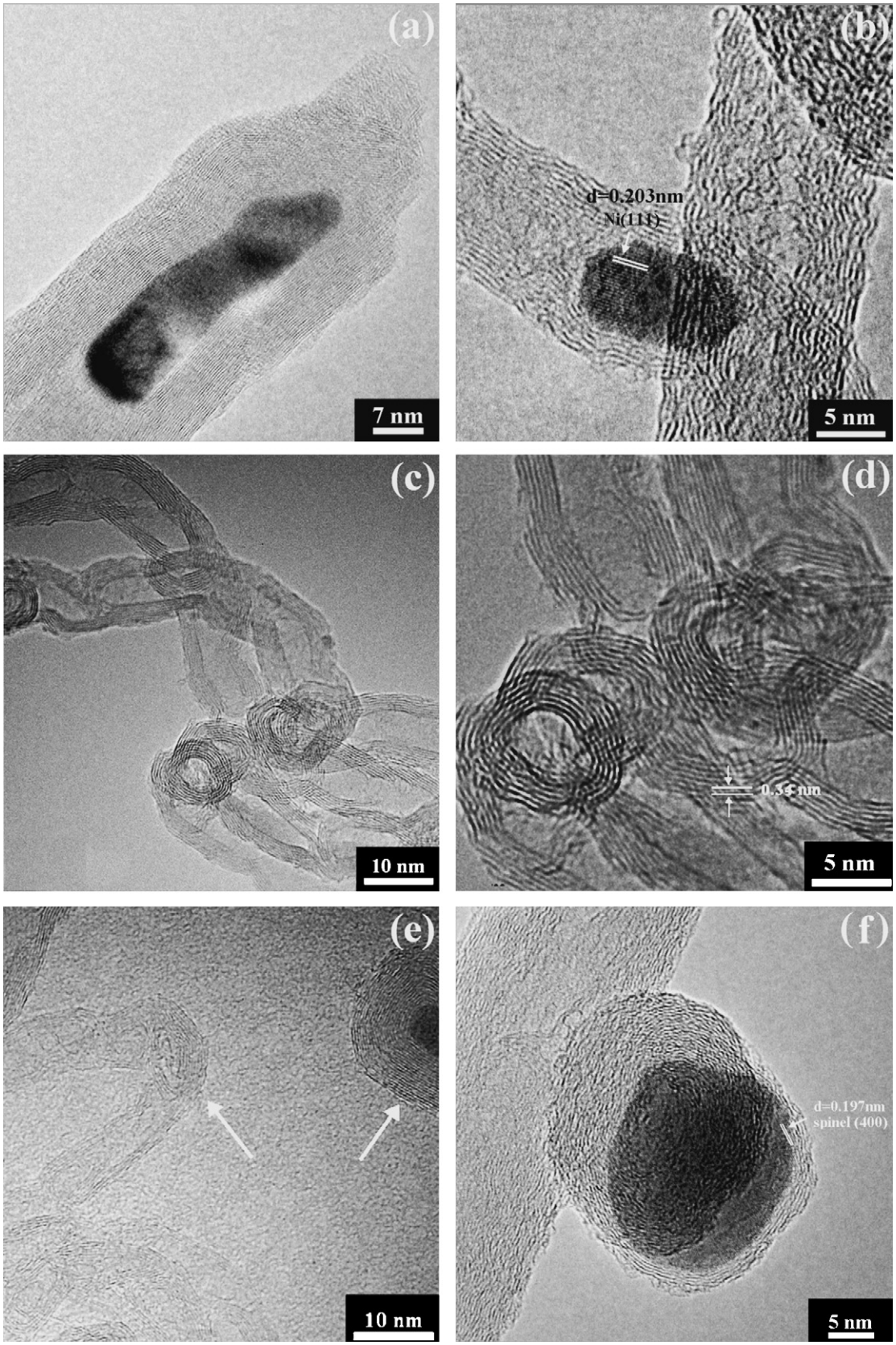

Fig. 8. HRTEM images of CNTs over calcined LDH-0.5: (a) image showing a slender catalyst particle at the end of nanotube and (b) image showing an elliptical catalyst particle along the radial direction inside the nanotube. HRTEM images of CNTs over calcined LDH-2: (c) image showing coiling of CNTs, (d) image showing an interlayer spacing of 0.34 nm for the (0 0 2) plane distance of graphite sheets, (e) image showing the zigzag node marked with left arrow and partial metal particle at the end of nanotube marked with right arrow and (f) image showing a spinel nanoparticle outside the nanotube.

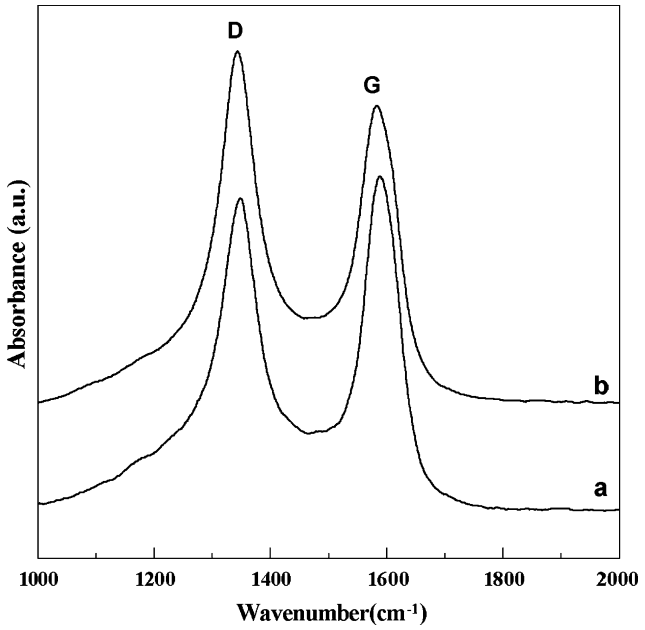

Fig. 9. Representative Raman spectra of CNTs over calcined LDH-0.5 (a) and LDH-2(b).

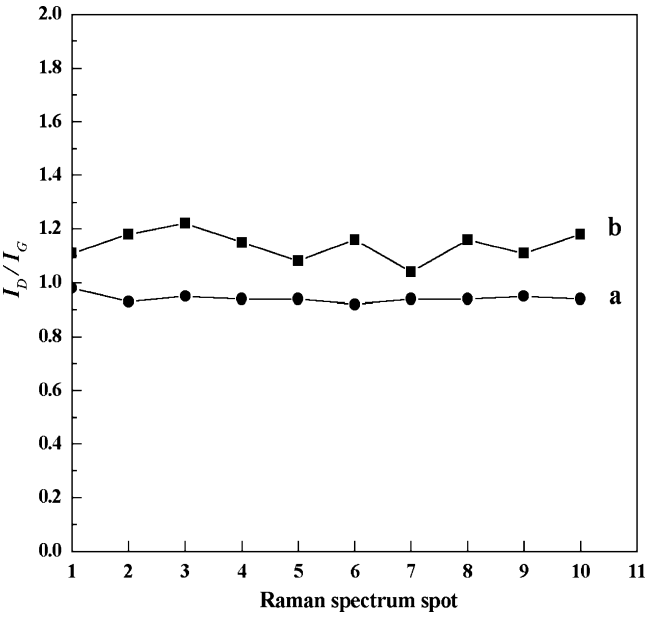

Fig. 10. The change curves of I_D/I_G values for carbon materials over calcined LDH-0.5 (a) and LDH-2 (b) with different Raman spectrum spots.

study is still required to clarify the inherent relationship between the structure and performance.

4. Conclusions

CNTs with straight and helical nanostructures have been grown over a series of catalysts derived from ternary Ni–Mg–Al LDH precursors prepared through the homogenous precipitation of urea under hydrothermal condition. The catalytically active Ni species for CNT growth were formed by calcining LDH precursors followed by an *in situ* reduction process. The results indicate that the carbon yield is enhanced with the increase of Mg content, owing to good dispersion of catalytically active Ni particles with small sizes. Further, the higher the Mg content, the more 3D-helical structured CNTs with different shapes including single-helical, planar-spiral and zigzag-like ones. It reveals that introduction of magnesium into catalysts has a distinct effect on the composition of catalysts and consequently on the structure of as-grown CNTs, and that the LDH precursor route to Ni-based supported catalyst may be advantageous to the preparation of straight and helical multi-walled CNTs in view of its characteristics of low cost, availability of highly dispersed catalytically active metal particles and tunable composition of catalysts.

Acknowledgements

We gratefully thank the financial support from the National Natural Science Foundation of China, 973 Program (2009CB939802), 111 Project (No. B07004) and Changjiang Scholars and Innovative Research Team in Universities (IRT 0406).

References

[1] S. Iijima, Nature 354 (1991) 56–58.
[2] A. Bachtold, P. Hadley, T. Nakanishi, C. Dekker, Science 294 (2001) 1317–1320.
[3] K.H. An, W.S. Kim, Y.S. Park, Y.C. Choi, S.M. Lee, D.C. Chung, D.J. Bae, S.C. Lim, Y.H. Lee, Adv. Mater. 13 (2001) 497–500.
[4] A. Javey, H. Kim, M. Brink, Q. Wang, A. Ural, J. Guo, P. McIntyre, P.M. Euen, M. Lundstrom, H. Dai, Nat. Mater. 1 (2002) 241–246.
[5] H.W. Zhu, C.L. Xu, D.H. Wu, B.Q. Wei, R. Vajtai, P.M. Ajayan, Science 296 (2002) 884–886.
[6] L.P. Zanello, B. Zhao, H. Hu, R.C. Haddon, Nano Lett. 6 (2006) 562–567.
[7] A. Volodin, D. Buntinx, M. Ahlskog, A. Fonseca, J.B. Nagy, C.V. Haesendonck, Nano Lett. 4 (2004) 1775–1779.
[8] X.Q. Chen, S. Motojima, H. Iwanaga, Carbon 7 (1999) 1825–1831.
[9] S. Ihara, S. Itoh, Carbon 33 (1995) 931–939.
[10] A.C. Dupuis, Prog. Mater. Sci. 50 (2005) 929–961.
[11] S.Y. Lee, M. Yamada, M. Miyake, Carbon 43 (2005) 2654–2663.
[12] S. Bhaviripudi, E. Mile, S.A. Steiner, A.T. Zare, M.S. Dresselhaus, A.M. Belcher, J. Am. Chem. Soc. 129 (2007) 1516–1517.
[13] D. Gournis, M.A. Karakassides, T. Bakas, N. Boukos, D. Petridis, Carbon 40 (2002) 2641–2646.
[14] V. Ivanov, J.B. Nagy, P.H. Lambin, A. Lucas, X.B. Zhang, X.F. Zhang, Chem. Phys. Lett. 223 (1994) 329–335.
[15] S. Amelinckx, X.B. Zhang, D. Bernaerts, X.F. Zhang, V. Ivanov, J.B. Nagy, Science 265 (1994) 635–639.
[16] H.Q. Hou, Z. Jun, F. Weller, A. Greiner, Chem. Mater. 15 (2003) 3170–3175.
[17] J.P. Cheng, X.B. Zhang, J.P. Tu, X.Y. Tao, Y. Ye, F. Liu, Mater. Chem. Phys. 95 (2006) 12–15.
[18] Y.K. Wen, Z.M. Shen, Carbon 39 (2001) 2369–2374.
[19] F. Cavani, F. Trifiro, A. Vaccari, Catal. Today 11 (1991) 173–301.
[20] D.G. Evans, X. Duan, Chem. Commun. 6 (2006) 485–496.
[21] D.G. Evans, R.C.T. Slade, Struct. Bond 119 (2006) 1–87.
[22] F. Li, X. Duan, Struct. Bond 119 (2006) 193–223.
[23] X.L. Liu, M. Wei, F. Li, X. Duan, AIChE J. 53 (2007) 1591–1600.
[24] H.I. Hima, X. Xiang, L. Zhang, F. Li, J. Mater. Chem. 18 (2008) 1245–1252.
[25] X. Xiang, L. Zhang, H.I. Hima, F. Li, D.G. Evans, Appl. Clay Sci. 42 (2009) 405–409.
[26] M. Bellotto, B. Rebours, O. Clause, J. Lynch, D. Bazin, E. Elkaim, J. Phys. Chem. 100 (1996) 8527–8534.
[27] X.D. Lei, F.Z. Zhang, L. Yang, X.X. Guo, Y.Y. Tian, S.S. Fu, F. Li, D.G. Evans, X. Duan, AIChE J. 53 (2007) 932–940.
[28] F. Millange, R.I. Walton, D. O'Hare, J. Mater. Chem. 10 (2000) 1713–1720.
[29] Y. Zhao, F. Li, R. Zhang, G.D. Evans, X. Duan, Chem. Mater. 14 (2002) 4286–4291.
[30] A. Vaccari, Catal. Today 41 (1998) 53–71.
[31] J.M. Fernández, M.A. Ulibarri, F.M. Labajos, V. Rives, J. Mater. Chem. 8 (1998) 2507–2514.
[32] R.B. Mathur, S. Seth, C. Lal, R. Rao, B.P. Singh, T.L. Dhami, Carbon 45 (2007) 132–140.
[33] Y. Abdi, J. Koohsorkhi, J. Derakhshandeh, S. Mohajerzadeh, H. Hoseinzadegan, Mater. Sci. Eng. C 26 (2006) 1219–1223.
[34] M.S. Dresselhaus, G. Dresselhaus, R. Saito, A. Jorio, Phys. Rep. 409 (2005) 47–99.
[35] M.S. Dresselhaus, G. Dresselhaus, A. Jorio, Annu. Rev. Mater. Res. 34 (2004) 247–248.
[36] J.W. Liu, M.W. Shao, Q. Xie, L.F. Kong, W.C. Yu, Y.T. Qian, Carbon 41 (2003) 2101–2104.
[37] S. Motojima, X. Chen, S. Yang, M. Hasegawa, Diamond Relat. Mater. 13 (2004) 1989–1992.
[38] S. Yang, X. Chen, S. Motojima, Diamond Relat. Mater. 13 (2004) 2152–2155.
[39] M. Lu, H.L. Li, J. Phys. Chem. B 108 (2004) 6186–6192.